Technical Report

TR-00-06

Behaviour of bentonite accessory minerals during the thermal stage

David Arcos, Jordi Bruno
Enviros-QuantiSci, Spain

Steven Benbow, Hiro Takase
Quintessa Ltd, United Kingdom

March 2000

Svensk Kärnbränslehantering AB
Swedish Nuclear Fuel
and Waste Management Co
Box 5864
SE-102 40 Stockholm Sweden
Tel 08-459 84 00
+46 8 459 84 00
Fax 08-661 57 19
+46 8 661 57 19

Behaviour of bentonite accessory minerals during the thermal stage

David Arcos, Jordi Bruno
Enviros-QuantiSci, Spain

Steven Benbow, Hiro Takase
Quintessa Ltd, United Kingdom

March 2000

Abstract

This report discusses in a quantitative manner the evolution of the accessory minerals in the bentonite as a result of the thermal event exerted by the spent fuel in the near field. Three different modelling approaches have been used and the results compared between them.

The three different approaches have been calculated using two Differential Algebraic Equation (DAE) solver: DYLAN (Model-1) and the Nag DAE solver, d02ngf (Model-2) and the third approach (Model-3) using the last version of PHREEQC.

The results from these calculations indicate the feasibility of the modelling approach to model the migration of bentonite accessory minerals and relevant aqueous species throughout the thermal gradient. These calculations indicate that the migration of quartz and quartz polymorphs is a lesser problem.

The aqueous speciation of Ca in the bentonite pore water is fundamental in order to define the potential migration of anhydrite during the thermal stage. If $CaSO_4(aq)$ is the predominant aqueous species, then anhydrite dissolves at the initial groundwater migration times through bentonite. However, if Ca^{2+} is considered to be the dominant Ca species at the bentonite pore water, then anhydrite migrates towards the clay/granite interface. This is the main difference in the chemical systems considered in the three model approaches used in this work.

The main process affecting the trace mineral behaviour in bentonite is cation exchange. This process controls the concentration of calcium, which results in a direct control of the calcite precipitation-dissolution.

Sammanfattning

Det här rapporten beskriver på ett kvantitativt sätt den geokemiska utvecklingen av föroreningsmineral i bentoniten som en följd av värmeproduktionen från det använda bränslet. Tre olika angreppssätt har använts och en jämförelse görs mellan de olika resultaten.

De tre olika angreppssätten har beräknats med två olika differentialekvationslösare (DAE): DYLAN (Modell-1) och Nag DAE lösaren d02ngf (Modell-2) och det tredje angreppssättet (Modell-3) använder den senaste versionen av PHREEQC.

Resultaten från beräkningarna visar tillämpbarheten av angreppssätten för att modellera migration av föroreningsmineral och relevanta lösta specier i en termisk gradient. Beräkningarna visar att migration av kvarts och kvartspolymorfer är ett underordnat problem.

Specieringen av Ca i bentonitens porvatten är fundamental för att definiera den potentiella migrationen av anhydrit i den termiska perioden. Om $CaSO_4(aq)$ är den dominerande specien, löser sig anhydriten när grundvatten kommer i kontakt med bentoniten. Om Ca^{2+} är dominerande sperien i porvattnet, kommer anhydriten att röra sig mot bentonit/berg gränsen. Detta är den huvudsakliga skillnaden mellan de kemiska systemen i de tre angreppssätten.

Den viktigaste processen som påverkar föroreningsmineralen i bentoniten är katjonbyte. Den processen kontrollerar koncentrationen av kalcium, vilken i sin tur styr upplösning/ utfällning av kalcit.

Table of contents

1 Introduction

SKB has selected MX-80 bentonite to be the barrier material in their engineered barrier system, hence the understanding of its behaviour is crucial. The long-term evolution of the accessory minerals is a key factor in the geochemical buffer capacity /Bruno et al, 1999/ and consequently in the physical properties of the bentonite. In this report we study the mineral alteration caused by the varying thermal gradients and the subsequent changing aqueous chemistry within the system.

This is done by using a chemical subset of the bentonite chemical model previously developed, which could in principle represent the main processes involved in the migration of the accessory minerals selected: carbonates (mainly calcite and siderite), sulphates (anhydrite), the quartz polymorphs (represented by different particle sizes) and cation exchange.

We compare the results from three different models using different computer approaches: two explicitly solving coupled reaction diffusion system using the Differential Algebraic Equation (DAE) solver DYLAN (Model-1) and the Nag DAE solver, d02ngf (Model-2), respectively; and the third approach (Model-3) using the last version of PHREEQC geochemical code /Parkhurst and Appelo,1999/.

In these models, the proposed spent fuel canister is represented as having an internal depth of 4.47m and an outer radius of 0.525m. The canister is assumed to be buried in granite inside a vertical hole, backfilled with compacted MX-80 bentonite to a thickness of 0.35 m. We model the 0.35 m clay buffer using a one-dimensional radially symmetric model (Model-2) the same is true for Model-1, except we used a bentonite width of 0.5m. Whereas for Model-3 a one-dimensional asymmetric granite plus bentonite (0.35 m width) model has been assumed. The model geometry is depicted in Figure 1-1.

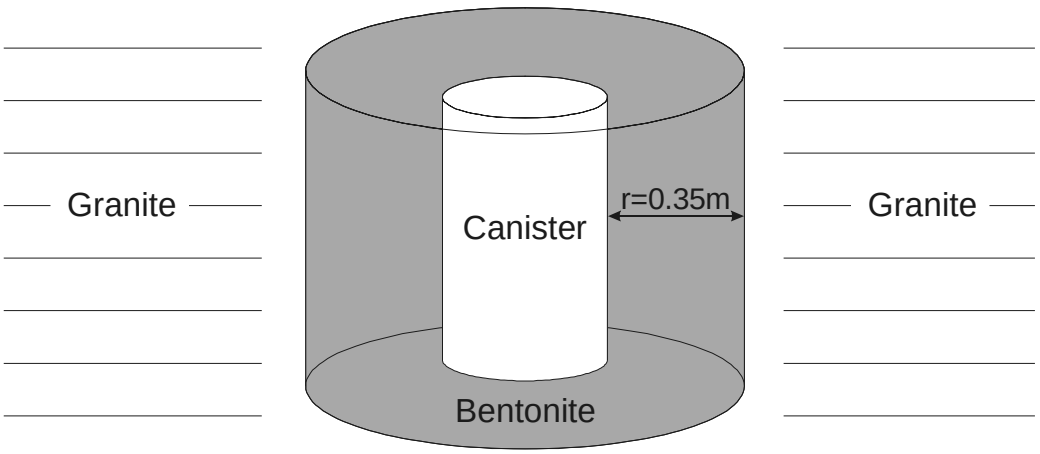

Figure 1-1. *Model geometry.*

2 Initial and boundary conditions considered in the models

The aim of this study is to investigate the effect of groundwater-bentonite interaction on the behaviour of accessory minerals and on the geochemical evolution of the system. As during the first thousand years the near field will be subjected to a thermal gradient due to the radioactive decay of the nuclear waste (up to 100ºC near the canister), the geochemical behaviour of the accessory minerals could introduce significant changes in the buffer capacity of the bentonite. For this reason, the model of the accessory mineral behaviour during this thermal period deserves a special attention. In order to select those parameters to be used in the models, first it is necessary to describe the main characteristics of the MX-80 bentonite.

Among the different descriptions found in the literature, the most careful and recent due is that of Madsen /1998/. Particularly, because in this work special attention is paid to the accessory mineral contents. The mineral content used in the different modelling approaches is shown in Table 2-1 and the Äspö granitic groundwater composition is shown in Table 2-2.

Table 2-1. Mineral composition of MX-80 bentonite used in the different approaches. Data for Model-1 and Model-3 from Madsen /1998/.

Mineral composition ($mol \cdot dm^{-3}$)		Model-1	Model-2	Model-3
Calcite		0.341	0.773	0.341
Siderite		0.295	0.662	0.295
Quartz		12.177	27.567	12.177
Anhydrite		0.122	0.276	0.122
Pyrite		n.c.	n.c.	0.013
Exchanger composition	NaX	n.c.	3.690	3.040
	KX	n.c.	n.c.	0.010
	CaX_2	n.c.	0.320	0.180
	MgX_2	n.c.	n.c.	0.073

n.c. not considered in the model.

Table 2-2. Äspö granitic groundwater composition.

Äspö groundwater composition (mol·dm-3)	
pH	7.7
pe	-4.5
Ca^{2+}	4.73·10-2
HCO_3^-	1.64·10-4
Fe^{2+}	4.30·10-6
H_4SiO_4	1.46·10-4
SO_4^{2-}	5.83·10-3
Cl^-	1.81·10-1
K^+	2.05·10-4
Mg^{2+}	1.73·10-3
Na^+	$9.13 \cdot 10^{-2}$

The thermal output of the spent fuel canister influences the aqueous chemistry through temperature-dependent variations in the equilibrium constants. Tarandi /1983/ carried out studies of the temperature in a repository, as a function of time after disposal. These calculations assumed an ambient temperature of 15°C, and some results are shown in Table 2-3. Repository temperatures that are estimated in these studies vary according to the type of model used and the assumptions made, particularly assumptions made on boundary conditions. For the purpose of this study an ambient temperature of 25°C is more realistic than 15°C. However, because of the ambiguities mentioned previously, the results of Tarandi for temperatures higher than 25°C will be used to model the temperature distribution. Another possibility would have been to use the results of Tarandi /1983/ for the temperature at the canister surface, as the near boundary condition in a near and far field model of the temperature distribution in the composite clay and rock domain. In this approach however, there is ambiguity in the assumed length of the rock domain. Too short a rock domain can lead to vastly lower temperatures than those of Tarandi /1983/, whilst too long a domain leads to far higher temperatures.

Table 2-3. Variation of canister and rock-bentonite interface temperature with time /Tarandi, 1983/.

Time after deposition (years)	Temperature (°C) at the bentonite-canister interface	Temperature (°C) at the bentonite-granite interface
40	80	65
100	78	70
1,000	60	58
5,000	45	44
10,000	35	35
50,000	25	25
100,000	18	18

Because of the slow rate of cooling of the canister, for Model-1 and Model-2 a pseudo steady state temperature model was used to simulate the temperature profile at each time step, and linear interpolation was used to estimate boundary temperatures as a function of time. The thermal conductivity of the bentonite that is assumed is based on the model developed by Knutsson /1983/. The thermal conductivity of saturated bentonite with a bulk density of 2.0-2.1 $g \cdot cm^{-3}$ is estimated to be 1.35-1.45 $W \cdot m^{-1} \cdot K^{-1}$ at 293K, and varies with temperature by approximately 0.1% per K. In the model the average value, 1.4 $W \cdot m^{-1} \cdot K^{-1}$ at 293K, is taken. For Model-3 a simple cooling approach with a thermal diffusion of 10^{-11} $m^2 \cdot s^{-1}$ has been applied in order to fit the temperature data from Tarandi /1983/.

There is little data available in the scientific literature on diffusion coefficients in bentonite for the aqueous species considered in this study, especially data at temperatures exceeding 25°C. The data found is summarised in Table 2-4.

According to the data from Table 2-4, we have observed that different parameters of the system can affect the diffusion coefficient value for a specific ion, leading to an apparent disagreement between the different experimental data. Among the different parameters affecting the diffusion coefficient values the ion type, the dry density value of the bentonite, the ionic strength, and the temperature are the most important ones.

Table 2-4. Diffusion coefficients in bentonite found in the literature.

Ion	Diffusion coefficient ($m^2 \cdot s^{-1}$) (Da)	Specials	Reference
H_2O	$3 \cdot 10^{-10}$	Dry density: 1.3 to 2.1 g/cm^3	Madsen /1998/
K^+	$5 \cdot 10^{-11}$	Dry density: 1.3 to 2.1 g/cm^3	Madsen /1998/
Fe^{2+}	$4 \cdot 10^{-11}$	Dry density: 1.3 to 2.1 g/cm^3	Madsen /1998/
Cl^-	10^{-10}	Dry density: 1.3 to 2.1 g/cm^3	Madsen /1998/
	$2 \cdot 10^{-10}$	Dry density: 1.16 g/cm^3	Kim et al /1993/
	$1.3 \cdot 10^{-10}$	Dry density: 1.36 g/cm^3	Kim et al /1993/
	$7.57 \cdot 10^{-11}$	Dry density: 1.58 g/cm^3	Kim et al /1993/
	$6 \cdot 10^{-12}$	Dry density: 1.82 g/cm^3	Kim et al /1993/
	$5.3 \cdot 10^{-12}$	Dry density: 1.9 g/cm^3	Kim et al /1993/
	$2 \cdot 10^{-11}$		Yu & Neretnieks /1997/
	$2 \cdot 10^{-11}$		Ochs /1997/
I^-	10^{-10}	Dry density: 1.3 to 2.1 g/cm^3	Madsen /1998/
	3.5 to $9.2 \cdot 10^{-11}$	Dry density: 1.8 g/cm^3, I = 0.018	Eriksen & Jansson /1996/
	$5 \cdot 10^{-11}$		Yu & Neretnieks /1997/
	$2 \cdot 10^{-11}$		Ochs /1997/
Sr^{2+}	$3 \cdot 10^{-11}$	Dry density: 1.3 to 2.1 g/cm^3	Madsen /1998/
	$1.1 \cdot 10^{-11}$	Dry density: 1.8 g/cm^3, I = 0.018	Eriksen & Jansson /1996/
	$1.7 \cdot 10^{-11}$	Dry density: 1.6 g/cm^3	Ramebäck et al /1994/
	$6.3 \cdot 10^{-12}$	Dry density: 2.1 g/cm^3	Ramebäck et al /1994/
	$2 \cdot 10^{-11}$ to $2 \cdot 10^{-12}$		Yu & Neretnieks /1997/
	$5 \cdot 10^{-12}$	Dry density: 1.8 g/cm^3	Muurinen et al /1994/
Na^+	$2 \cdot 10^{-10}$	Dry density: 1.8 g/cm^3, 10000ppm Na, 25°C	Pusch et al /1989/
	$5 \cdot 10^{-11}$	Dry density: 1.8 g/cm^3, 100ppm Na, 25°C	Pusch et al /1989/
	10^{-10}	Dry density: 1.8 g/cm^3, 10000ppm Na, 90°C	Pusch et al /1989/
	$4 \cdot 10^{-12}$	Dry density: 1.8 g/cm^3	Muurinen et al /1994/

Although, we have not found much data at temperatures higher than 25°C, it seems that this parameter does not affect in a significant way the diffusion coefficient value (see the case for sodium as an example). For this reason we have considered to use the same diffusion coefficient values at 100 °C than at 25 °C. On the other hand, the effect of the specific ion concentration, the ionic strength, and the bentonite density are more critical parameters affecting the diffusion coefficient.

The only relevant diffusion coefficient from this study however is that of Fe^{2+}, which Madsen found to have a diffusion coefficient of $4 \cdot 10^{-11}$ $m^2 \cdot s^{-1}$ in bentonite at 25 °C with dry density 1.3-2.1 $g \cdot cm^{-1}$. Many aqueous species, for example K^+, Cl^-, I^-, Sr^{2+} and Na^+, have been found to have diffusion coefficients varying between 10^{-10} to 10^{-11} $m^2 \cdot s^{-1}$ in bentonite with similar dry densities. In the model we take the most conservative of these values (the largest) as the diffusion coefficient for each of the aqueous species other than Fe^{2+}.

2.1 Model-1

The accessory minerals under consideration are the carbonates (calcite and siderite), quartz and anhydrite described by the precipitation and dissolution reactions,

$$\text{Calcite} + H^+ = Ca^{2+} + HCO_3^-$$
$$\text{Siderite} + H^+ = Fe^{2+} + HCO_3^-$$
$$\text{Quartz} + 2H_2O = H_4SiO_4$$
$$SiO_2(am) + 2H_2O = H_4SiO_4$$
$$\text{Anhydrite} = Ca^{2+} + SO_4^{2-}$$

Quartz was chosen to be representative of all of the silica phases. From the set of reactions, we identify 4 minerals and 6 aqueous species to be modelled, namely the minerals, calcite, siderite, quartz and anhydrite, and the aqueous species H^+, Ca^{2+}, HCO_3^-, Fe^{2+}, H_4SiO_4 and SO_4^{2-}. We use the notation m_i (mol·dm^{-3}) to describe the concentration of each mineral species and a_j (mol·dm^{-3}) to describe the concentration of each aqueous species, where the subscripts *i* and *j* are described in Table 2-5.

Table 2-5. Mineralogical and aqueous species notation used in the Model-1.

Species	Abbreviation
Calcite	m_1
Siderite	m_2
Quartz	m_3
Anhydrite	m_4
H^+	a_1
Ca^{2+}	a_2
HCO_3^-	a_3
Fe^{2+}	a_4
H_4SiO_4	a_5
SO_4^{2-}	a_6

The logarithm of the temperature-dependent equilibrium constants, K_1, K_2, K_3 and K_4 for the carbonates, quartz and anhydrite reactions (where the subscripts '1', '2', '3' and '4' correspond to the calcite, siderite, quartz and anhydrite reactions respectively) can be fitted to the degree four polynomial equation

$$\log K_i\,(T) = A_i + B_iT + C_iT^2 + D_iT^3 + E_iT^4$$

where T is the temperature (°C) and the constants A_i, B_i, C_i, D_i, and E_i are given in Table 2-6.

Table 2-6. A_i, B_i, C_i, D_i, and E_i values for the calculation of the solubility constant as a function of temperature.

Mineral	A_i	B_i	C_i	D_i	E_i
Calcite	2.21136	$-1.4467\cdot10^{-2}$	$-3.1977\cdot10^{-6}$	$6.9908\cdot10^{-8}$	$-2.0819\cdot10^{-10}$
Siderite	0.29929	$-2.0260\cdot10^{-2}$	$2.4590\cdot10^{-5}$	$-6.9130\cdot10^{-9}$	$-1.2473\cdot10^{-10}$
Quartz	-4.50772	$2.3001\cdot10^{-2}$	$-1.1467\cdot10^{-4}$	$3.3332\cdot10^{-7}$	$-3.8136\cdot10^{-10}$
Anhydrite	-4.06197	$-8.1476\cdot10^{-3}$	$-7.1226\cdot10^{-5}$	$2.5351\cdot10^{-7}$	$-4.7998\cdot10^{-10}$

For the near canister boundary condition we specify that the spatial derivative of each aqueous species is zero, i.e.

$$\frac{\partial a_i}{\partial x} = 0, \quad i = 1,\text{K},6$$

that means the initial pore water in the bentonite is distilled water which is allowed to equilibrate with the minerals present in the bentonite.

At the bentonite rock boundary we specify that the aqueous species concentrations are the same as that of the granitic groundwater composition of Äspö (Table 2-2).

In the model, we will assume that the dissolution-precipitation of the carbonates and anhydrite are governed by instantaneous equilibrium conditions, whilst the dissolution-precipitation of quartz is driven by kinetics. The methods of modelling these types of reaction are described in the following subsections.

2.1.1 Instantaneous equilibrium

Instantaneous equilibrium assumptions are used to describe the dissolution-precipitation of calcite, siderite and anhydrite. Considering the calcite dissolution-precipitation reaction motivates the method of modelling these reactions,

$$\text{Calcite} + H^+ = Ca^{2+} + HCO_3^-$$

The activity product for the calcite reaction, Q_1, is given by

$$Q_1 = \frac{\left[Ca^{2+}\right]\left[HCO_3^-\right]}{\left[H^+\right]}$$

and the instantaneous equilibrium assumption implies that wherever calcite is present in the domain, the concentrations of the aqueous species satisfies the equation

$$Q_1 = K_1(T) \tag{2-1}$$

and in this case we say that the activity product, Q_1, lies on the equilibrium manifold for the calcite reaction. The concentration of calcite can be calculated from the change in the aqueous species concentrations. Subject to the constraint (2-1), the aqueous species are also free to diffuse within the groundwater, so that

$$\frac{\partial a_j}{\partial t} = \nabla \cdot \left(D_i \nabla a_j \right) \quad j = 1,2,3 \tag{2-2}$$

Whenever there is no calcite present the aqueous ions are able to diffuse, without being affected by the chemical reactions, within the groundwater (unless subject to further equilibrium constraints by other instantaneous mineral reactions), and Q_1 is allowed to deviate from the equilibrium manifold.

If the initial mineral and aqueous species concentrations do not satisfy the equilibrium constraints, a fast reaction must take place to move the system to the equilibrium conditions. The only exception to this case occurs when the calcite concentration is zero, and the activity product is smaller than the reaction rate, mathematically when $m_1 = 0$ and $Q_1 < K_1(\mathrm{T})$. In this case no calcite precipitation occurs, and the aqueous species are free to diffuse within the groundwater. The equations used to model these initial fast reactions are based on the type of rate equations found, for example, in Rimstidt and Barnes /1980/. The rate of calcite dissolution-precipitation, R_1 (mol·dm^{-3}·s^{-1}), is given by

$$\begin{aligned} \frac{\partial m_1}{\partial t} &= R_1, \\ \frac{\partial a_j}{\partial t} &= \nabla \cdot \left(D_j \nabla a_j \right) - n_{1,j} R_1, \qquad j = 1,2,3, \\ R_1 &= \begin{cases} 0, & m_1 = 0 \text{ and } Q_1 < K(T), \\ \mu_1 \left(\dfrac{Q_1}{K_1(T)} - 1 \right), & \text{otherwise}, \end{cases} \end{aligned} \tag{2-3}$$

where μ_1 is a large (possibly temperature dependent) prescribed reaction rate constant (in the model we take μ_1 = 106 mol·dm^{-3}·s^{-1}), $n_{1,j}$, j =1,2,3 depend on the stoichiometry of the calcite reaction and D_j is the diffusion coefficient of aqueous species a_j in bentonite. If the system is initially over-saturated with aqueous species, $Q_1 \geq K_1(\mathrm{T})$, then $R_1 > 0$ and calcite is precipitated, calcite dissolution occurs if the reverse is true. This equation holds until Q_1 meets the equilibrium manifold, after which time equation (2-1) governs the evolution of the system. The equilibrium manifold approach is summarised in Table 2-7. It should be noted that the above derivation is based upon a single reaction. With the inclusion of further reactions, additional reaction terms must be included in equation (2-3) and additional constraint equations, analogous to equation (2-1), must be formed.

Table 2-7. Summary of the equilibrium manifold equations for the single instantaneous reaction.

Situation	**Governing Equations**
$m_1 > 0$ and $Q_1 = K_1(\mathrm{T})$	**(2-1) and (2-2)**
$m_1 > 0$ and $Q_1 \neq K_1(\mathrm{T})$ or $m_1 = 0$ and $Q_1 \geq K_1(\mathrm{T})$	(2-3) with $R_1 = \begin{cases} 0, & m_1 = 0 \text{ and } Q_1 < K(T), \\ \mu_1 \left(\dfrac{Q_1}{K_1(T)} - 1 \right), & \text{otherwise}, \end{cases}$
$m_1 = 0$ and $Q_1 < K_1(\mathrm{T})$	(2-3) with $R_1 = 0$

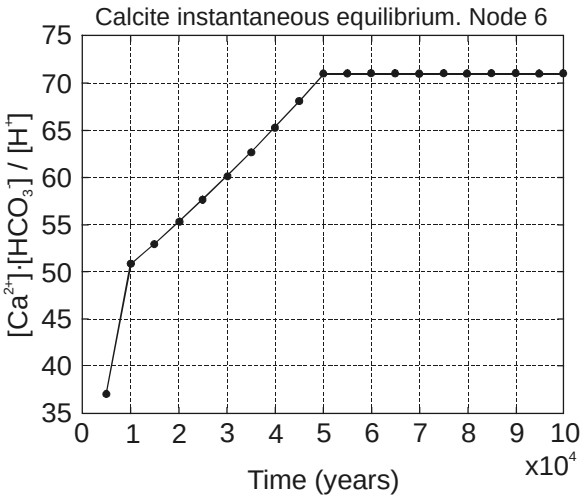

Figure 2-1. *Adherence of the activity product to the equilibrium manifold. Dots indicate variation of $K_1(T)$ with time. Solid curve traces the activity product, Q_1.*

The adherence of the activity product to the equilibrium manifold is demonstrated in Figure 2-1. As can be seen, for this particular node in the domain, the activity product Q_1 lies on the equilibrium manifold described by $K_1(T)$ for the entire evolution of the system, which indicates that calcite is always present at this node. The initial fast reaction that moves the system into equilibrium is too fast to appear on this scale.

2.1.2 Quartz kinetics

It is assumed that quartz dissolution and precipitation reactions are continually competing in the reaction

$$\text{Quartz} + 2H_2O = H_4SiO_4$$

Based on existing rate laws for quartz dissolution at fixed temperatures and experimental results, Tester et al /1994/ derived an expression for the rate of quartz dissolution, R_+ (mol·dm^{-3}·s^{-1}), as a function of temperature. It was found that,

$$R_+ = Ak_f(T) \tag{2-4}$$

where A (m^2·dm^{-3}) is the relative interfacial area between the solid and aqueous phases. Tester et al. gave the following formula for $k_f(T)$ (mol·m^{-2}·s^{-1}),

$$k_f(T) = (276 \pm 193)\exp(-90.1(\pm 2.5)/RT)$$

where T is the temperature in Kelvin and R is the gas constant. To calculate the relative surface area, A, in (2-4) it is necessary to know the grain size of quartz, d(m). Then given that the molecular mass of quartz is 0.06 kg·mol^{-1} and assuming a quartz density of 2.65 kg·dm^{-3}, the relative surface area of quartz is given by

$$A = \frac{0.06}{1000 \times 2.65}\left(\frac{6}{d}\right)m_3 \tag{2-5}$$

where, as in Table 2-5, m_3 is the concentration of quartz (mol·dm^{-3}).

The precipitation reaction $R\_$ (mol·dm^{-3}·s^{-1}), is assumed to satisfy

$$R_{\_} = Ak_r(T)[\mathrm{H_4SiO_4}] \tag{2-6}$$

Here A is as in equation (2-4), and $k_r(T)$ is given by,

$$k_r(T) = 136.77\exp(-66.076/RT)$$

In order to calculate $k_r(T)$ we have calculated the H_4SiO_4 concentration at saturation as a function of the temperature following the equation /Tester et al, 1994/:

$$\log m^{sat}_{H4SiO4} = A + B\cdot\log V + C\cdot(\log V)^2$$

where V is the specific volume of pure water (cm^3·g^{-1}) and A, B, and C are empirical temperature-dependent constants given by:

A = -4.66206 + 0.0034063·T + 2179.7·T^{-1} - 1.1292·106·T^{-2} + 1.3543·108·T^{-3}
B = -0.0014180·T - 806.97·T^{-1}
C = 3.9465·10-4·T

where T is the absolute temperature in Kelvin.

According to these data we have calculated the k_f-value and the silica concentration at saturation at different temperatures, so we can calculate the k_r-values at these temperatures. We fitted these values by using an equation of the same type as this one used for calculating the k_f-value as a function of temperature (Figure 2-2).

The total quartz reaction is then described by,

$$\begin{aligned} \frac{\partial m_3}{\partial t} &= R_3, \\ \frac{\partial a_5}{\partial t} &= \nabla\cdot(D_5\nabla a_5) - n_{3,5}R_3, \end{aligned} \tag{2-7}$$

where the total reaction rate $R_3 = R_+ - R\_$.

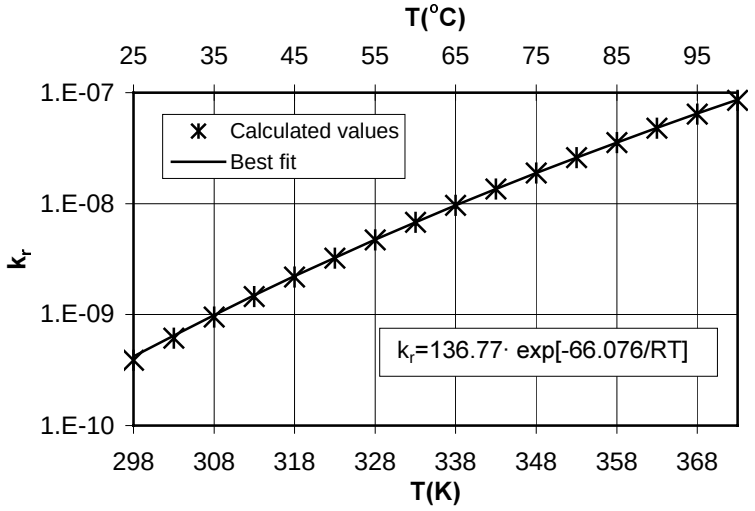

Figure 2-2. *k_r-values vs. Temperature calculated by using data from Tester et al /1994/, and best fit for these data.*

2.1.3 System of equations

Using equations (2-1), (2-2), (2-3) and (2-7), the evolution of the concentrations of aqueous species and minerals in the instantaneous carbonate and anhydrite reactions and quartz reaction can be summarised by the system of equations,

$$\frac{\partial a_i}{\partial t} = \nabla \cdot \left(D_i \nabla a_i \right) - \sum_{j=1}^{4} n_{j,i}^{*} R_j, \quad i = 1,\text{K},6,$$

where $n_{j,i}^{*}$ is equal to the stochiometry of aqueous species i in reaction j if reaction j is *not* in instantaneous equilibrium, otherwise $n_{j,i}^{*}$ is zero; and (2-8)

$$\frac{\partial m_j}{\partial t} = R_j \quad \text{or } Q_j = K_j(T), \quad j = 1,\text{K},4,$$

depending on whether reaction j is in instantaneous equilibrium.

Equation (2-8) can be rewritten as

$$\begin{bmatrix} & M_1 & \\ \cdots & \cdots & \cdots \\ & M_2\left(a_1,\text{K},a_6,m_1,\text{K},m_4\right) & \end{bmatrix} \begin{bmatrix} \dot{a}_1 \\ \text{M} \\ \dot{a}_6 \\ \cdots \\ \dot{m}_1 \\ \text{M} \\ \dot{m}_4 \end{bmatrix} = \begin{bmatrix} \nabla \cdot \left(D_1 \nabla a_1 \right) \\ \text{M} \\ \nabla \cdot \left(D_6 \nabla a_6 \right) \\ \cdots \\ f\left(a_1,\text{K},a_6,m_1,\text{K},m_4,T\right) \end{bmatrix} \tag{2-9}$$

Here $M_1 \in \Re^{6x10}$ is a matrix, which combines the aqueous species and mineral equations to cancel the stoichiometric factors in the aqueous species equations. The matrix $M_2 \in \Re^{4x10}$ and vector f describe the equilibrium manifold constraints and mineral time derivative terms. Equation (2-9) is in a form that allows numerical discretisation of the system to be solved by a standard Differential Algebraic Equation solver, such as the QuantiSci DYLAN solver.

2.2 Model-2

This model is based on Model-1 but modified by adding the cation exchange process and the species $CaSO_4$ to the aqueous species set.

Another difference is that the former model was discretised in a way suitable for solution with the Differential Algebraic Equation (DAE) solver DYLAN. Whereas in the present model we used the Nag DAE solver, d02ngf, one of the suite of numerical methods in the Nag Fortran Library, which is based on the SPRINT DAE solver /Berzins and Furzeland, 1985/.

Although most of the parameters and boundary conditions of the model are the same than in Model-1, some differences have been considered. Initial water compositions are slightly different to Model-1 as shown in Tables 2-2 and 2-8. The Äspö water corresponds to the incoming groundwater at the granite/bentonite interface and the MX-80 water is assumed to be the initial bentonite pore water.

Table 2-8. MX-80 bentonite pore water composition for Model-2.

Bentonite pore water composition ($mol \cdot dm^{-3}$)	
pH	7.0
Ca^{2+}	$2.15 \cdot 10^{-3}$
HCO_3^-	$7.79 \cdot 10^{-2}$
Fe^{2+}	$2.10 \cdot 10^{-8}$
H_4SiO_4	$9.35 \cdot 10^{-5}$
SO_4^{2-}	$1.30 \cdot 10^{-1}$
Cl^-	$6.40 \cdot 10^{-3}$
K^+	$3.29 \cdot 10^{-4}$
Mg^{2+}	$1.52 \cdot 10^{-3}$
Na^+	$4.14 \cdot 10^{-1}$

Also mineral compositions have been changed and additional data on the concentrations of exchangeable cations have been considered (Table 2-1). The cation exchange reaction is considered to be an instantaneous equilibrium reaction with a temperature-independent equilibrium constant as there are no data for temperatures above 25°C. The selected constants for the exchange reactions are from Olin et al /1995/.

2.3 Model-3

As previously indicated, this model has been calculated using the last version of PHREEQC geochemical code /Parkhurst and Appelo,1999/. In this version diffusion and mixed diffusion-advection can be considered in transport calculations instead of pure advection, also variations in temperature can be considered, allowing to perform a geochemical simulation in a more complete fashion of the near field evolution. The bentonite has been divided in different cells (up to 7 cells in this case, of 5 cm each cell) and a total time calculation of 100,000 years has been considered. In this new model aqueous components diffuse through the cells reacting with the accessory bentonite minerals and exchangeable cation sites of the clay. Also a temperature evolution has been considered for the whole system in each cell (Figure 2-3).

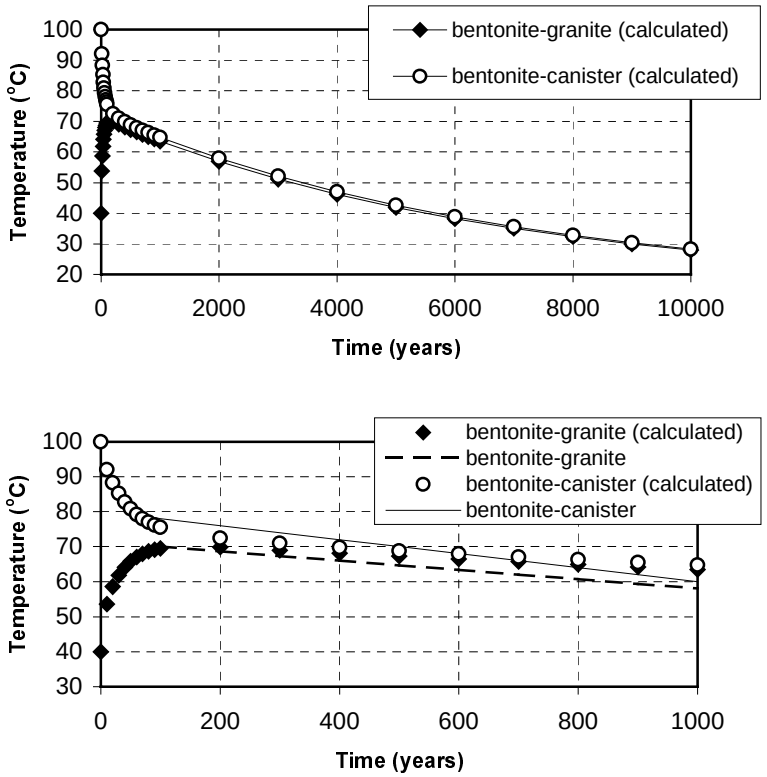

Figure 2-3. *Temperature evolution in the bentonite-canister and bentonite-granite boundaries for Model-3. Temperatures calculated by Tarandi /1983/ at both bentonite ends have also been plotted in the graphic up to 1,000 years for comparison (normal and dashed lines).*

The system that is considered in this model has some differences relative to Model-1 and Model-2. Some of these differences are due to a refinement of the initial parameters, whereas others are due to the capabilities of the code itself.

The waters considered in this model are presented in Tables 2-2 and 2-9. The Äspö groundwater is the same than in the previous models, whereas the initial MX-80 pore water has important differences relative to Model-2. This bentonite pore water is considered to be distilled water in equilibrium with the bentonite according to the methodology used in Bruno et al /1999/. Slight differences between calculated pore water in Bruno et al /1999/ and the one presented here are due to differences in the initial accessory mineral composition of the MX-80 bentonite, as we selected here the one from Madsen /1998/ as shown in Table 2-1. It is important to note that pyrite equilibrium has been considered in Model-3, and also that the activity of $CaSO_4$(aq) is smaller than in Model-2.

Table 2-9. MX-80 bentonite pore water composition for Model-3.

Bentonite pore water composition ($mol \cdot dm^{-3}$)	
pH	7.0
pe	3.3
Ca^{2+}	$1.00 \cdot 10^{-4}$
HCO_3^-	$2.95 \cdot 10^{-3}$
Fe^{2+}	$6.06 \cdot 10^{-7}$
H_4SiO_4	$3.48 \cdot 10^{-4}$
SO_4^{2-}	$4.20 \cdot 10^{-2}$
Cl^-	$2.00 \cdot 10^{-3}$
K^+	$7.20 \cdot 10^{-5}$
Mg^{2+}	$6.54 \cdot 10^{-5}$
Na^+	$8.00 \cdot 10^{-2}$

The differences existing between the accessory mineral content relative to one litre of pore water are related to the difference in the bentonite density and its porosity. For Model-3 we selected a bentonite density of $2.0 g \cdot cm^{-3}$ and a pore water/bentonite ratio of 0.41 at the repository conditions according to Bruno et al /1999/.

The temperature-dependence of the equilibrium constants for dissolution and speciation reactions have been approximated by the following virial expression, as considered in the PHREEQC geochemical code /Parkhurst and Appelo,1999/:

$$\log K(T) = A + BT + \frac{C}{T} + D \log T + \frac{E}{T^2}$$

where T is the temperature in Kelvin. Quartz is considered to be in thermodynamic equilibrium, which implicitly considers a fast and reversible dissolution/precipitation. This is because the calculated differences are very small when considering kinetics and it was observed that quartz was close to equilibrium in the system. Only cation exchange reactions have been considered to be temperature-independent reactions due to the lack of data above 25°C selecting the constant values from Olin et al /1995/.

The transport calculations have been performed considering a 1D diffusion model, with a diffusion coefficient of $10^{-11} m^2 \cdot s^{-1}$ for all aqueous species, which is one order of magnitude smaller than the diffusion coefficients assumed in Model-1 and 2. Although for comparison a set of calculations have been carried out for Model-3 using the same diffusion coefficients than for Model-1 and 2 (see below).

An additional major difference between Model-3 and the previous ones is that in Model-3 an extra cell of granite is considered at the bentonite/granite interface. This has been done to allow the granite to be heated and thus change the thermal evolution of the system to fit the values from Tarandi /1983/. In any case, water in this cell has not been allowed to equilibrate with any solid phase.

3 Results

3.1 Model-1

Using DYLAN, the system described in equation (2-10) was discretised and solved for Quartz grain sizes of 10 μm, 100 μm and 1mm. The spatial profile of each mineral and aqueous species was discretised using 12 nodes, giving a spatial resolution of 4.167 cm. Adaptive time stepping is handled internally by DYLAN, and simulations were run for 100,000 years.

3.1.1 Equilibrium manifold adherence

Figure 3-1 demonstrates the behaviour of the activity products for the instantaneous equilibrium reactions. As can be seen in this figure the calcite activity product, Q_1, at a point in the clay buffer that is approximately 23 cm from the canister (node 6) lies on the equilibrium manifold for the entire evolution of the system. This implies that a non-zero calcite concentration is present at this node for the entire evolution, as will be seen in Figure 3-3 (in fact calcite is present across the whole domain for the entire evolution, but in varying amounts). Similar behaviour can be observed for the anhydrite reaction in Figure 3-1. The behaviour of the siderite reaction is somewhat different. Figure 3-1 indicates that, at node 1, which is approximately 2.1 cm from the canister, siderite is present for the entire 100,000 years. However, it can be seen that, at node 5 (18.75 cm from the canister), the activity product Q_2 only lies on the equilibrium manifold for approximately 95,000 years. After this time the activity product moves away from the equilibrium manifold, which indicates that all the siderite at this node has dissolved by approximately 95,000 years. Looking further along the domain, away from the canister, it can be seen that at node 12 (approximately 2.1 cm from the bentonite-rock interface), the siderite reaction is only in instantaneous equilibrium for a very short time (too short a time to be resolved at this scale). These observations are consistent with the concentrations of the aqueous species that are relevant to the siderite reaction, as will be discussed in the sequel.

3.1.2 Anhydrite precipitation

Before studying the evolution of the carbonates and the aqueous species relevant to these reactions, a note must first be made about the anhydrite concentration. It can be seen from Figure 3-2 that the anhydrite concentration grows very quickly at the bentonite-rock interface. In fact, the anhydrite reaction is so fast that the pore space available for anhydrite precipitation is entirely used up in the first 261 years. Because the current model only takes account of clay chemistry, and not clay porosity structure, there is no mechanism by which the anhydrite precipitation can be stopped. One possibility is to apply a precipitation limit to the anhydrite reaction, which effectively switches off the anhydrite precipitation reaction when all of the available pore space is used up. In such a model however, the incoming Ca^{2+} and SO_4^{2-} ions would then quickly diffuse through the precipitated anhydrite and further precipitation would occur adjacent to the existing anhydrite. A wave of anhydrite precipitation would then work its way towards the canister. This behaviour is unrealistic, since a large deposit of anhydrite

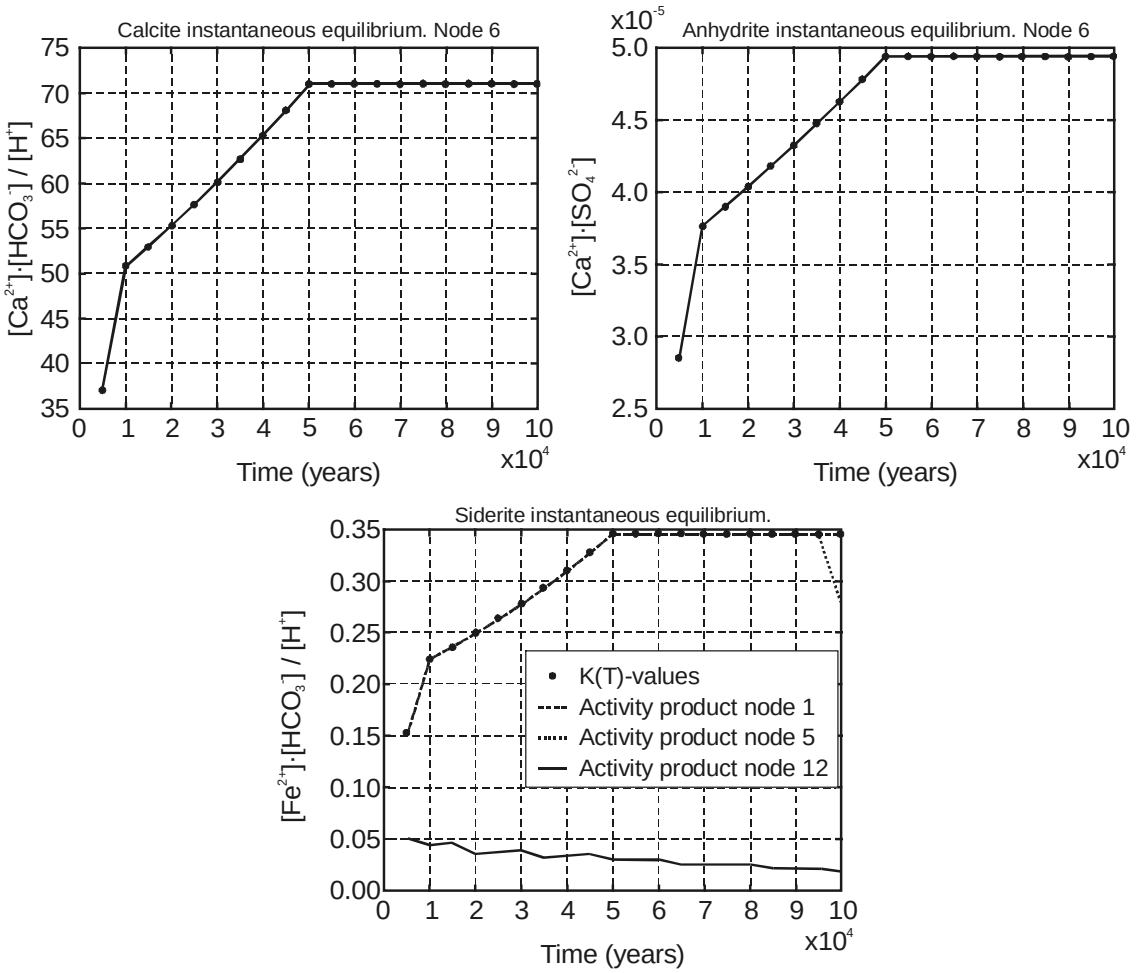

Figure 3-1. *Instantaneous equilibrium for calcite and anhydrite at node 6 and for siderite at nodes 1, 5 and 12. K(T)-values are marked with dots, whereas curves stand for activity products.*

filling all of the available pore space at the bentonite-rock interface would reduce the rate of diffusion of aqueous ions into the system, thereby greatly reducing the rate at which anhydrite could propagate towards the canister. Instead, the model ignores any increase in anhydrite concentration once the pore-space is filled. Ignoring the anhydrite reaction has the effect of limiting the in-diffusion of Ca^{2+} and SO_4^{2-} ions, which is more physically realistic; a large build-up of anhydrite at the rock-bentonite interface would reduce the inflow of each aqueous species into the clay. Ignoring the anhydrite reaction in the model however, only accounts for a reduced rate of flow of Ca^{2+} and SO_4^{2-}. Hence to improve the model the coupled clay chemistry and pore structure should be modelled, but this is beyond the scope of this work. The impact of these observations is not expected to be great since, as will be seen, the majority of the aqueous species are held in instantaneous equilibrium everywhere in the domain, and when in instantaneous equilibrium the concentrations of the aqueous species are relatively insensitive to the boundary conditions. Boundary concentrations can differ from interior concentrations by orders of magnitude.

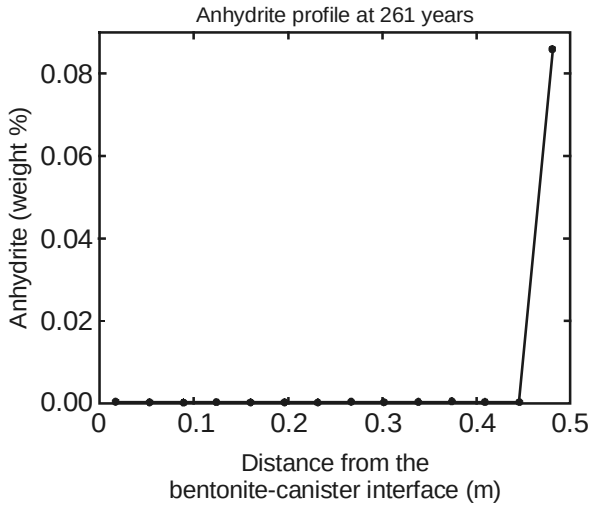

Figure 3-2. *Graph showing the anhydrite precipitation at the bentonite-granite interface after 261 years.*

3.1.3 Calcite and siderite travelling waves

The calcite and siderite weight percentages of the total solid mass are 0.7%. The behaviour of the carbonates, calcite and siderite, and the ions Ca^{2+} and Fe^{2+} over the first 100,000 year-period is shown in Figure 3-3. Initially, at t = 0,

$$Q_1 = 388.78, \quad K_1 = 18.75$$
$$Q_2 = 0.035, \quad K_2 = 0.12$$

so that $Q_1 > K_1$ and calcite is precipitated, and $Q_2 < K_2$ hence siderite is dissolved. The initial Ca^{2+} decreases to support the calcite precipitation. Whilst the Fe^{2+} concentration increases with the siderite dissolution. These changes are approximately uniform across the domain, with Ca^{2+} concentration decreasing from 0.047 $mol \cdot dm^{-3}$ to approximately 0.042 $mol \cdot dm^{-3}$, and the relatively more significant change in Fe^{2+} concentration increasing from $4.3 \cdot 10^{-6}$ $mol \cdot dm^{-3}$ to around $2 \cdot 10^{-4}$ $mol \cdot dm^{-3}$.

After these initial fast changes, which have only a small effect on the carbonate weight percentages, some more dramatic behaviour occurs. As the canister cools, the temperature at the clay-rock interface also falls and $K_1(T)$ and $K_2(T)$ both begin to increase. To remain in instantaneous equilibrium then, both calcite and siderite activity products must increase. One mechanism by which this might occur is that the calcite and siderite concentrations both decrease. However, what in fact happens is that siderite dissolution takes place to such an extent that the siderite is totally dissolved near the bentonite-rock boundary, and the spare HCO_3^- ions are used in the calcite reaction to balance the equilibrium constraint so that calcite is actually precipitated. As can be seen in Figure 3-3, the calcite concentration at the bentonite-rock interface increases to approximately 1.3% of the total solid weight, whilst the siderite concentration there decreases to zero.

As the canister continues to cool we see, in Figures 3-3 that a wave of calcite precipitation and siderite dissolution sweeps across the domain driven by the exchange of HCO_3^- ions. Due to the limited supply of HCO_3^- ions by siderite dissolution, the calcite concentration is limited to approximately 1.3% of the total solid weight. The speed of the dissolution-precipitation wave over time is plotted in Figure 3-4. As can be seen, the speed of the wave is fastest initially at around $6.75 \cdot 10^{-6}$ $m \cdot year^{-1}$ when the bentonite is

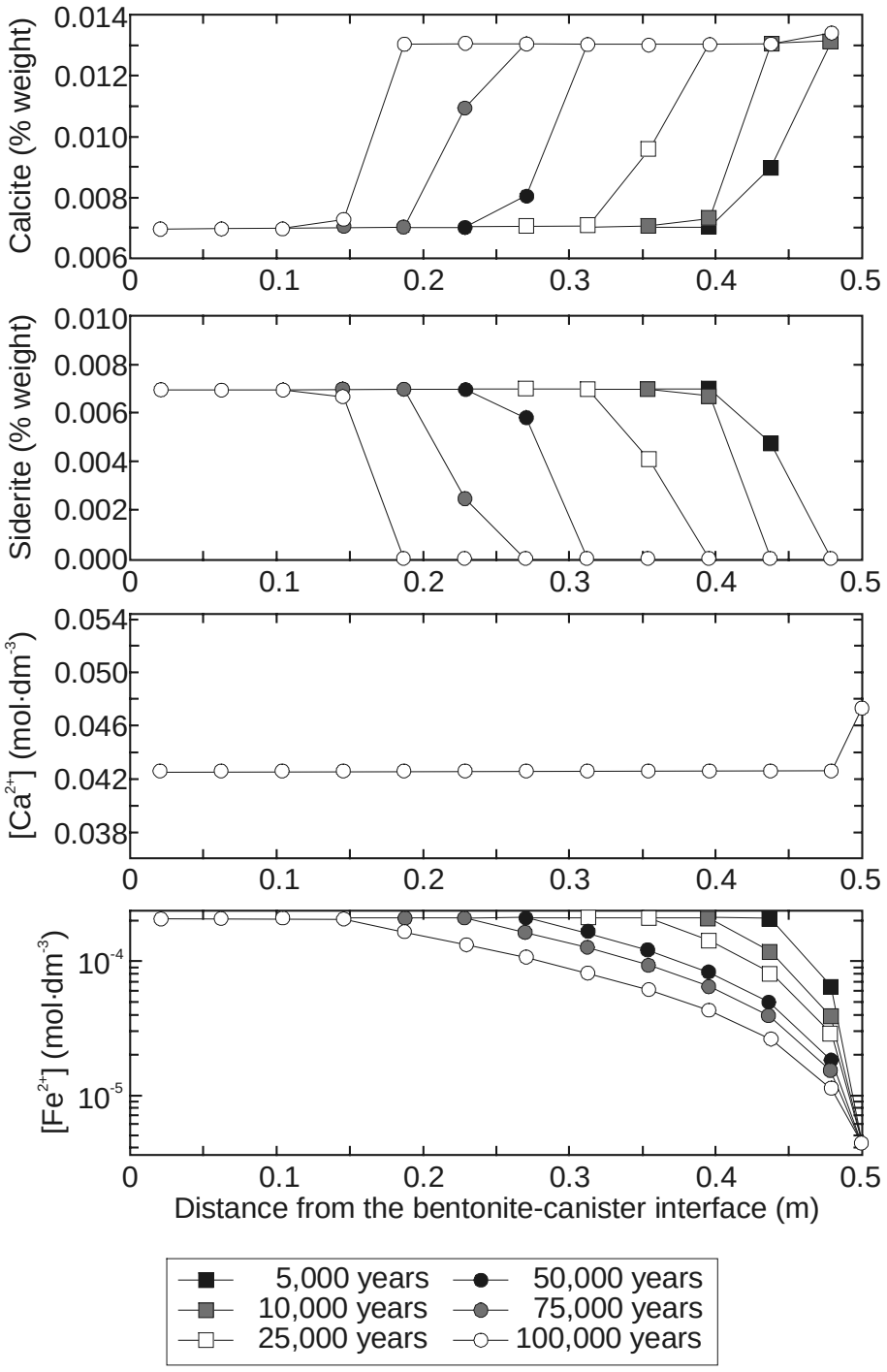

Figure 3-3. *Evolution of calcite, siderite and the concentrations of Ca^{2+} and Fe^{2+} in the Model-1.*

hot, and slows to around $2.25 \cdot 10^{-6}$ m·year^{-1} as the bentonite cools. Taking $2.25 \cdot 10^{-6}$ m·year^{-1} as the wave speed that prevails after 100,000 years, and assuming that the wave has a further 0.175 m to travel to reach the canister, we can estimate the time taken for the wave to travel across the entire bentonite region to be a further 77,777 years. Thus we expect that after 177,777 years, the siderite inventory in the bentonite will have expired and an approximately uniform calcite mass of 1.3% the initial solid mass will be present in the clay.

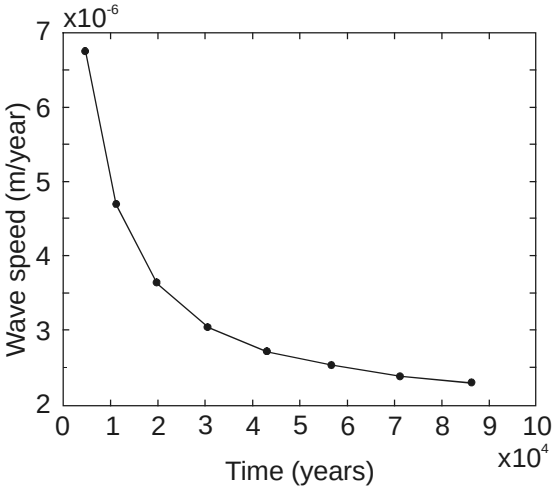

Figure 3-4. *Variation of carbonate travelling wave speed with time.*

As calcite is present everywhere in the domain for the entire 100,000 years evolution, the H^+, Ca^{2+} and HCO_3^- concentrations are constrained by the equilibrium manifold conditions. Since the mechanism by which calcite propagates and siderite vanishes across the domain is the exchange of free HCO_3^- ions, the concentrations of each of the aqueous species just mentioned are almost uniform across the domain, temperature variation across the domain making little difference to the spatial profile. Only at the boundaries do these aqueous species show any spatial behaviour, where it can be seen that the Äspö groundwater boundary conditions differ from the equilibrium conditions in the domain considered here, other than for the Ca^{2+} and HCO_3^- concentrations which agree fairly closely. pH is virtually neutral in the MX-80 bentonite compared to 7.7 in Äspö water, and SO_4^{2-} concentration is approximately 5 times lower here than in Äspö. The only aqueous species free from the equilibrium constraints is Fe^{2+} which is diffusion dominated behind the wave front (where no siderite is present).

3.1.4 Results of quartz reactions

The quartz reaction is dependent on the quartz grain size (see equation (2-4)). Quartz grain sizes of d = 10 μm, 100 μm and 1 mm where taken, and the results are plotted in Figure 3-5 for the case d = 10 μm, Figure 3-6 for d = 100 μm and Figure 3-7 for d = 1mm.

Case d = 10μm

Since the quartz reaction rate is dependent on the reciprocal of the grain size, the smaller grain sizes give rise to the fastest reactions. As can be seen from the H_4SiO_4 concentration profile at 5,000 years (Figure 3-5), there is an initial increase in the H_4SiO_4 concentration across the domain, with the resulting interior concentrations in the bentonite being higher than the corresponding Äspö boundary condition. This is due to quartz dissolution, which is initially greatest at the (hot) canister boundary. After a short time however, the H_4SiO_4 concentration at the bentonite-rock boundary becomes relatively small (since it is fixed at Äspö H_4SiO_4 concentration), which results in reduction of the quartz precipitation rate, R_- at this boundary. The total quartz reaction rate, R_3 then becomes dominated by the quartz dissolution reaction, R_+, and the quartz begins to

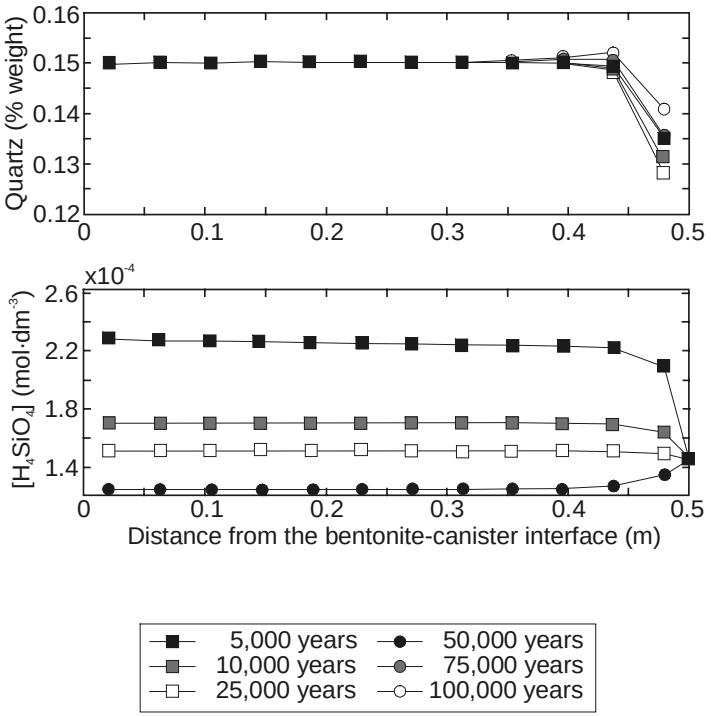

Figure 3-5. *Evolution of Quartz and H_4SiO_4 concentration for Model-1 and quartz grain size of 10 μm.*

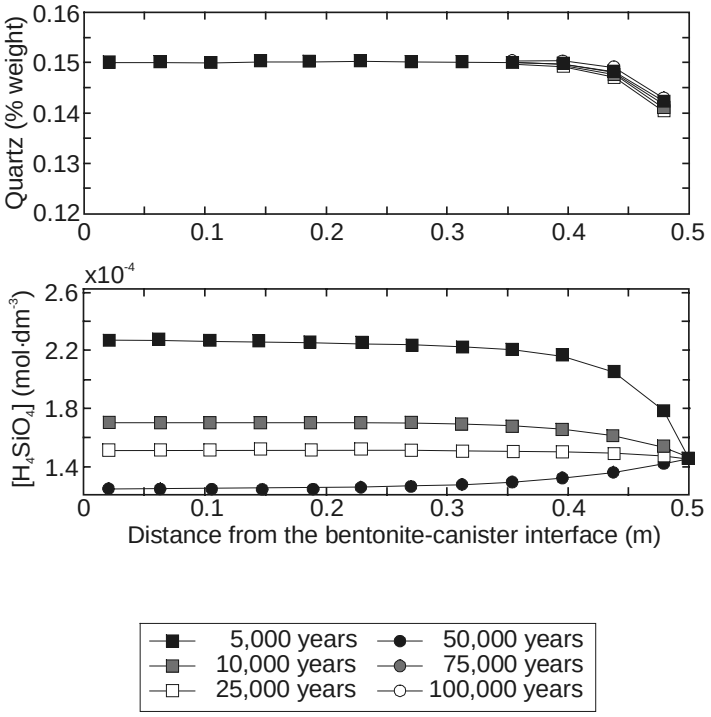

Figure 3-6. *Evolution of Quartz and H_4SiO_4 concentration for Model-1 and quartz grain size of 100 μm.*

dissolve more quickly at this end of the domain. After approximately 25,000 years the temperature has reduced sufficiently for the quartz precipitation reaction to dominate the dissolution reaction at the bentonite–rock boundary, and quartz precipitation begins. At this time the quartz mass at this interface is at a minimum of around 12.8% of the total solid mass (from an initial amount of 15% of the total solid mass), and the H_4SiO_4 concentration is close to a uniform value equal to the Äspö H_4SiO_4 concentration.

After 25,000 years, quartz is precipitated fastest in the bentonite at node 11 (6.25 cm from the bentonite-rock interface), where the low temperature, but still relatively high H_4SiO_4 concentration, cause the precipitation reaction $R\_$ to dominate the dissolution reaction R_+ to the greatest extent. Quartz precipitation is slow adjacent to the bentonite-rock interface because of the low temperature (even though the H_4SiO_4 concentration here is highest). After 100,000 years the quartz occupies approximately 15% of the solid mass in the region up to 35 cm from the canister. The mass then increases to a peak of around 15.2% of the solid mass at a distance of 6.25 cm from the bentonite-rock interface, before falling to around 14% of the solid mass at a distance of 2.1 cm from the interface.

Case d = 100 μm

For this case, and indeed for the case d = 1mm, the overall behaviour is qualitatively similar to the case of the smaller grain size, but quantitatively less significant due to the reduced reaction rates (Figure 3-6). There is an initial period, during which quartz dissolution takes place, which lasts for between 5,000 and 10,000 years. After this time the quartz mass is reduced by only a small amount across the majority of the domain, but is reduced from 15% of the solid mass to 14% of the solid mass at the node nearest the clay-rock interface. After this dissolution phase, quartz precipitation begins at a slow rate. After the 100,000-year evolution, the final maximum quartz mass is 15.03% of the solid mass between 31.25-35.42 cm from the canister. The minimum quartz mass again appears at the bentonite-rock interface where the low temperature gives rise to small precipitation rates, and a final quartz mass of 14.25% of the total solid mass.

Case d = 1mm

Figure 3-7 shows the quartz behaviour for d = 1mm. As can be seen, there is very little quartz dissolution, the greatest amount occurring again at the bentonite-rock interface, where the quartz mass is reduced to around 14.8% of the total solid mass. Very little quartz precipitation occurs after this time.

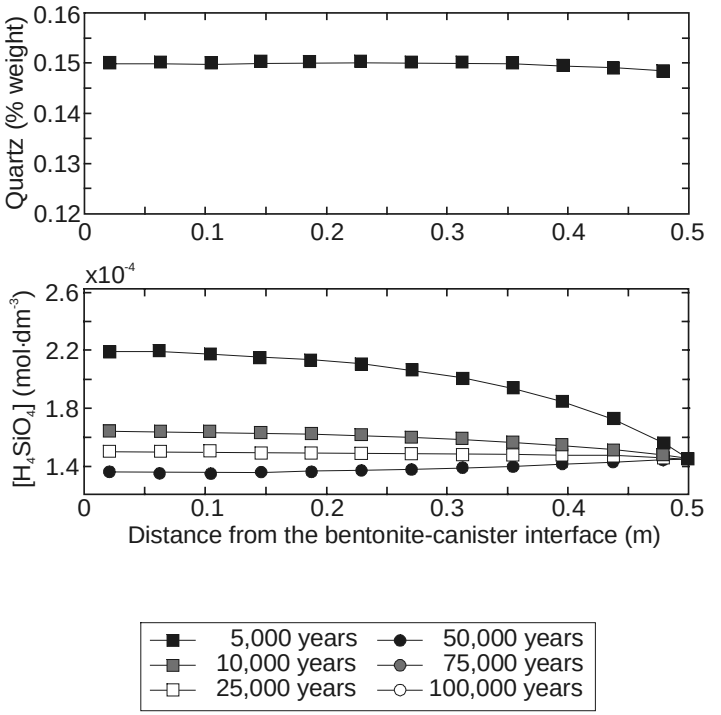

Figure 3-7. *Evolution of Quartz and H_4SiO_4 concentration for Model-1 and quartz grain size of 1 mm.*

3.2 Model-2

The initial concentrations of aqueous $CaSO_4$ in the Äspö and MX-80 pore waters is very similar ($5.39 \cdot 10^{-2}$ mol·dm^{-3} and 5.4710^{-2} mol·dm^{-3} respectively). However, after the initial equilibration phase, its concentration in the buffer is reduced, so that the incoming Äspö pore water has a higher concentration of $CaSO_4$ (Figure 3-8). To maintain the instantaneous equilibrium conditions in the buffer, this incoming $CaSO_4$ readily breaks down to Ca^{2+} and SO_4^{2-} ions, thus increasing the concentrations of these species in the system. The heightened concentrations Ca^{2+} and SO_4^{2-} then cause increased anhydrite precipitation at the rock/clay interface (Figure 3-9). The rate of anhydrite precipitation is

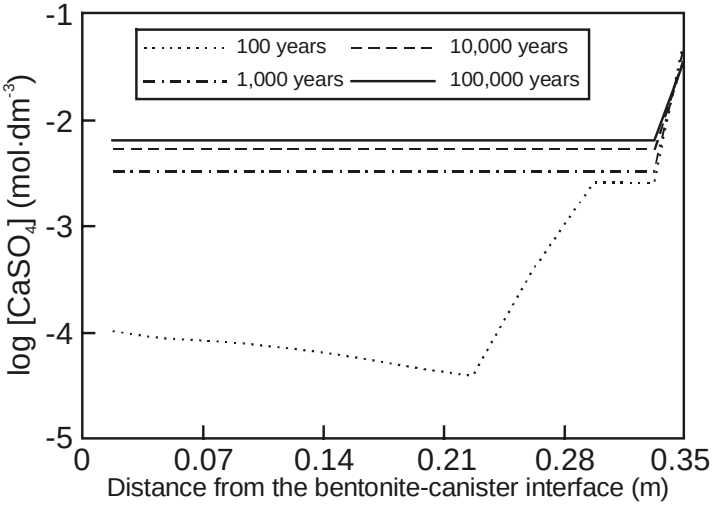

Figure 3-8. *Evolution of aqueous $CaSO_4$ concentration in Model-2.*

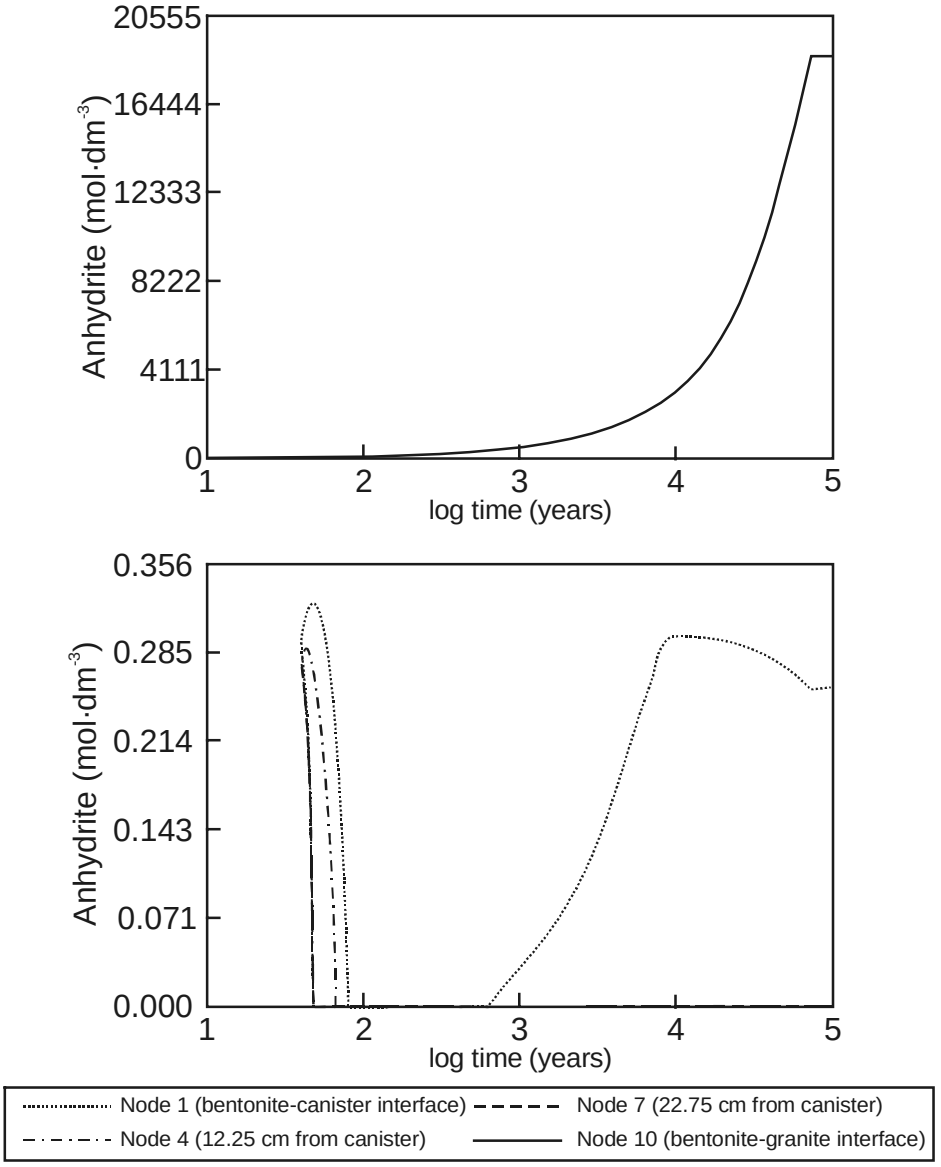

Figure 3-9. *Anhydrite evolution at the granite-bentonite interface (above) and in the interior of the buffer (below) for Model-2.*

increased to approximately seven times that in Model-1. Thus the inclusion of the $CaSO_4$ aqueous species actually enlarges the anhydrite precipitation effect at the bentonite/granite interface.

As in the previous calculations of Model-1 an increase in the calcite content of bentonite has been observed through the bentonite buffer. This increase of calcite is favoured by the siderite dissolution (Figure 3-10).

Another important aspect is the replacement of Na by Ca at the bentonite exchange sites, which is totally achieved before 1,000 years (Figure 3-11).

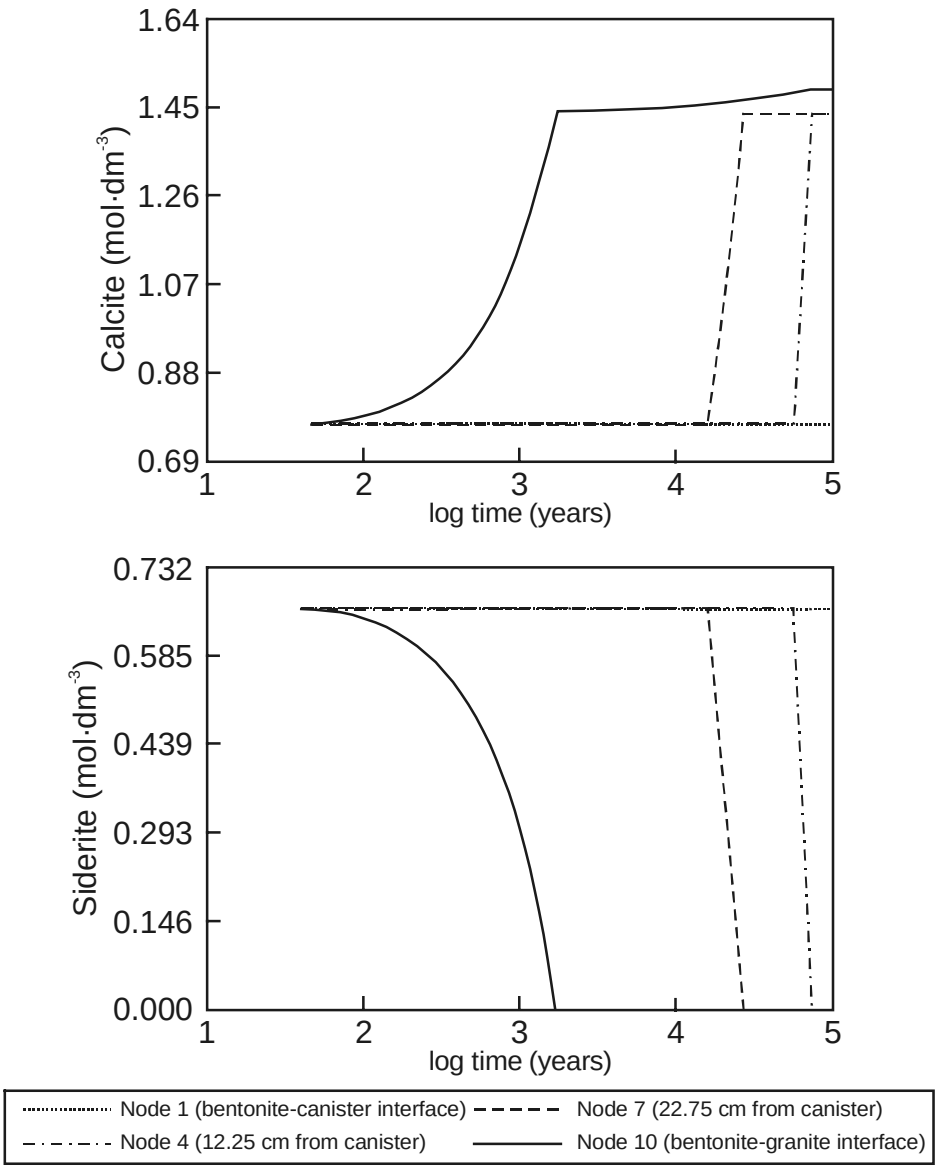

Figure 3-10. *Calcite and siderite evolution for Model-2.*

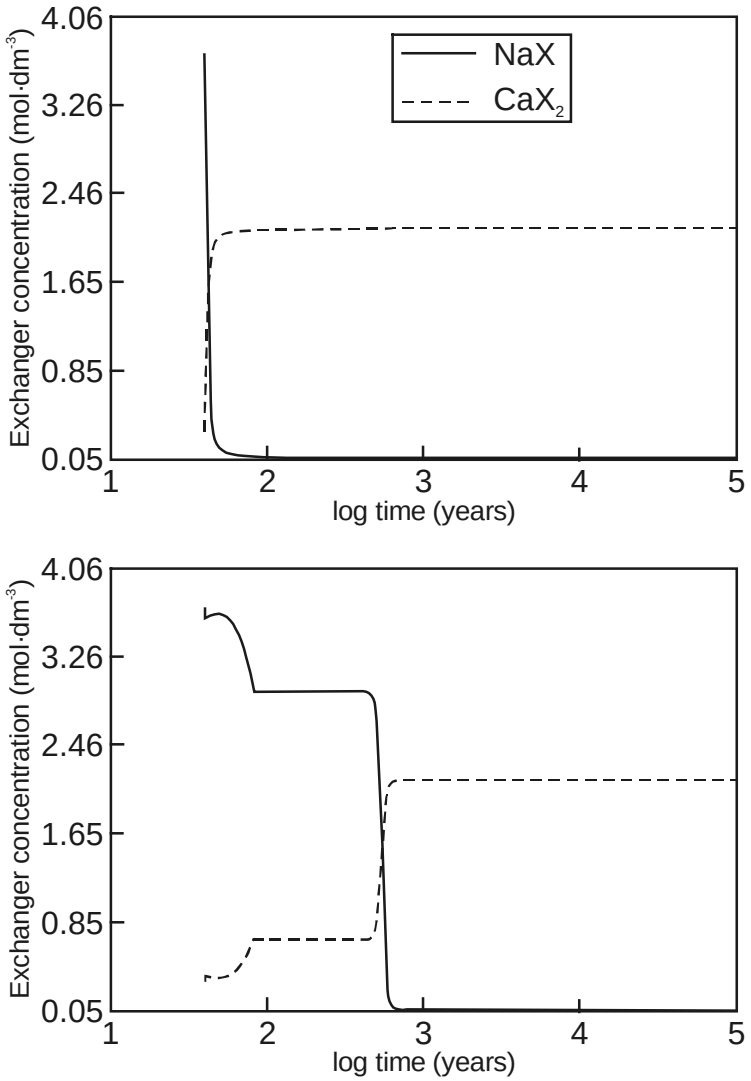

Figure 3-11. *NaX and CaX_2 concentrations at the granite-bentonite interface (above) and at bentonite-canister interface (below) for Model-2.*

3.3 Model-3

The results from this model are not very different from those obtained in Bruno et al /1999/. The main differences are related to the effect of considering diffusion instead of pure advection.

In this model the driving process is also the cation exchange process, which consumes most of the calcium excess, hampering the precipitation of calcite. Na^+ mainly replaces Ca^{2+} in the bentonite exchange sites, while Mg^{2+} only replaces 4 to 6% of the initial Na^+ sites. Interestingly enough the replacement by K^+ is negligible throughout the simulation. As the ion exchange process proceeds (Figure 3-12), the Ca^{2+} available for calcite precipitation increases, resulting in calcite precipitation. This effect is more evident close to the granite/bentonite boundary (Figure 3-13), where replacement of Ca^{2+} by Na^+ occurs to a higher degree. Notice that in Model-3, the cation exchange reaction traverses the system at a greatly reduced rate than that in Model-2. In Model-2, the cation exchange reaction is exhausted by 1,000 years when all of the possible exchange sites

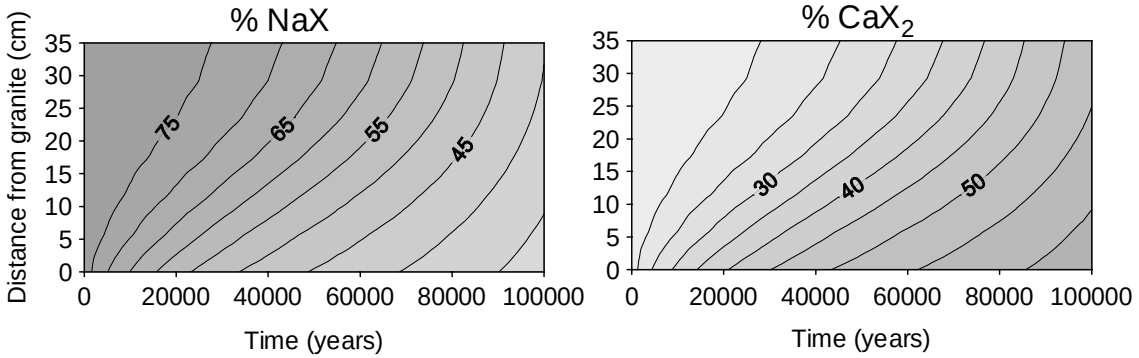

Figure 3-12. *Percentage of occupancy of the exchangeable cation site by Na and Ca in Model-3.*

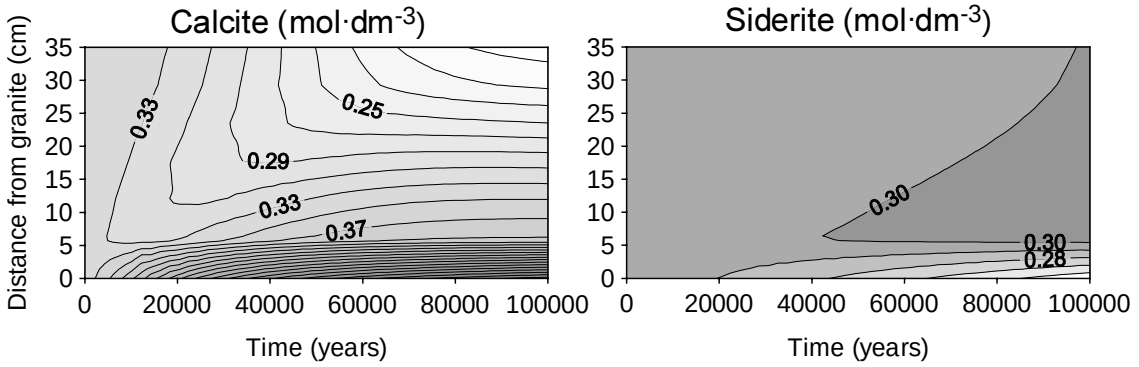

Figure 3-13. *Amounts of calcite and siderite remaining in bentonite for Model-3.*

had been used up, whereas in Model-3, the cation reaction is still occurring at 100,000 years. This is mainly a consequence of considering a lower diffusion coefficient for Model-3. The precipitation of calcite is also enhanced by the dissolution of siderite close to the granite, being an additional source for aqueous carbonate.

The generalised dissolution of calcite that occurs in the centre of the bentonite buffer and close to the canister is a consequence of the carbonate diffusion to the host rock. The HCO_3^- concentration in the Äspö groundwater is around one order of magnitude lower than in the MX-80 pore water, thus the diffusion of bicarbonate from bentonite to the granite causes a decrease of calcite saturation index in the bentonite system (Figure 3-14). On the other hand, the two-order of magnitude difference in the calcium concentration between Äspö groundwater and MX-80 pore water causes a diffusion of Ca^{2+} to

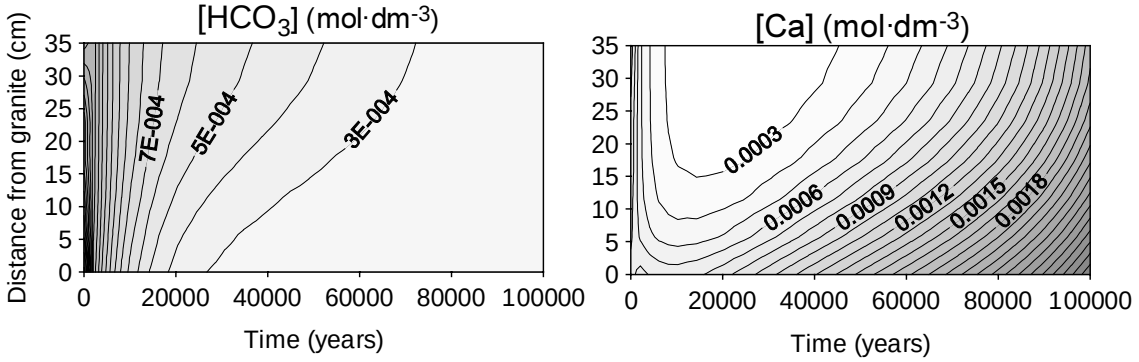

Figure 3-14. *Evolution of the concentration of aqueous carbonate and calcium in Model-3.*

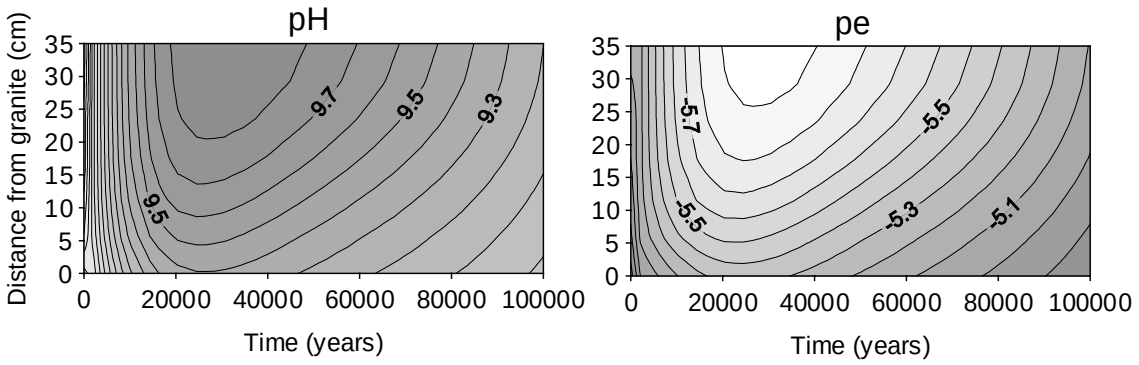

Figure 3-15. *pH and pe evolution in Model-3.*

the bentonite. In any case, as the cation exchange process consumes most of the calcium, its diffusion does not causes an increase in the calcite saturation index to compensate its decrease produced by the diffusion of bicarbonate (Figure 3-14).

On the contrary, the higher concentration of iron in Äspö groundwater, which also causes a diffusion of iron from the granite to the bentonite, maintains the siderite saturation index close to equilibrium in most of the bentonite system. Only where calcite precipitates the decrease in aqueous carbonate causes the dissolution of siderite.

As indicated in Bruno et al /1999/ the pH of the system is buffered by the equilibrium with calcite, thus the 7.7 pH of Äspö groundwater rises up to values between 9.1 and 9.8 (Figure 3-15). The redox buffer in the system is exerted by the Fe(II)-Fe(III) pair, represented by the siderite and pyrite equilibria, maintaining the pe to reducing conditions (Figure 3-15). Only up to a 0.3% of pyrite is dissolved in the bentonite close to the Äspö granite.

The problem related to the anhydrite increase in Model-1 and 2 here disappears as anhydrite dissolves completely at the initial times of the calculations. To explain the difference in the anhydrite behaviour between the present model and the previous ones, we must refer to the aqueous calcium and sulphate evolution.

In Model-1 the aqueous species SO_4^{2-} and Ca^{2+} were the only ones considered for aqueous sulphate and calcium respectively. If under the range of chemical conditions of the model there were other aqueous species, different than aqueous SO_4^{2-} and Ca^{2+}, predominating in the sulphate and/or calcium speciation, this could explain the different behaviour of anhydrite in the system.

In the present model aqueous SO_4^{2-} is the predominant aqueous species of sulphate, accounting for around 75% of the sulphate in solution. Thus sulphate speciation is not the responsible of the different behaviour of anhydrite. On the other hand, the aqueous speciation of calcium changes during the geochemical evolution of the system. At the beginning of the calculations aqueous $CaSO_4$ is the predominant species, whereas as the system evolves Ca^{2+} increases up to be the dominant species after than around 10,000 years (Figure 3-16).

This difference in the calcium speciation could be the reason for the difference in the anhydrite behaviour between Model-3 and Model-1. As in Model-1 aqueous $CaSO_4$ was not considered, then the amount of Ca^{2+} was larger than the corresponding one, increasing the anhydrite saturation index up to be oversaturated.

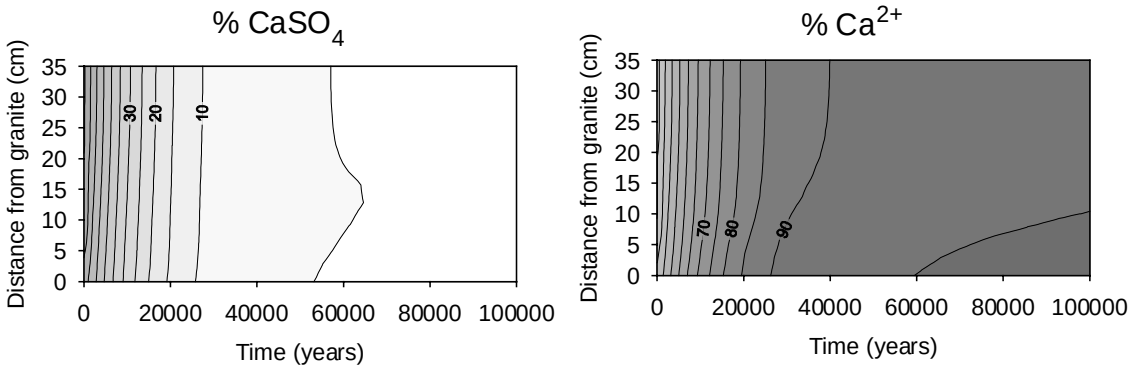

Figure 3-16. *Aqueous calcium dominant species in Model-3.*

Another possible source for the discrepancy could be due to some differences in the initial conditions of the calculations. It is reasonable to think that as Model-2 and Model-3 use different initial conditions (water compositions, diffusion coefficients, and mineral amounts), the results could not be totally comparable. For this reason we have calculated a second Model-3 up to 1,000 years, using the same conditions than in Model-2. In this case, anhydrite also dissolves completely at later times (Figure 3-17). Anyway, the reason for anhydrite dissolution is the same as for the original Model-3; this is the predominance of aqueous $CaSO_4$ over Ca^{2+} as it is shown in Figure 3-17.

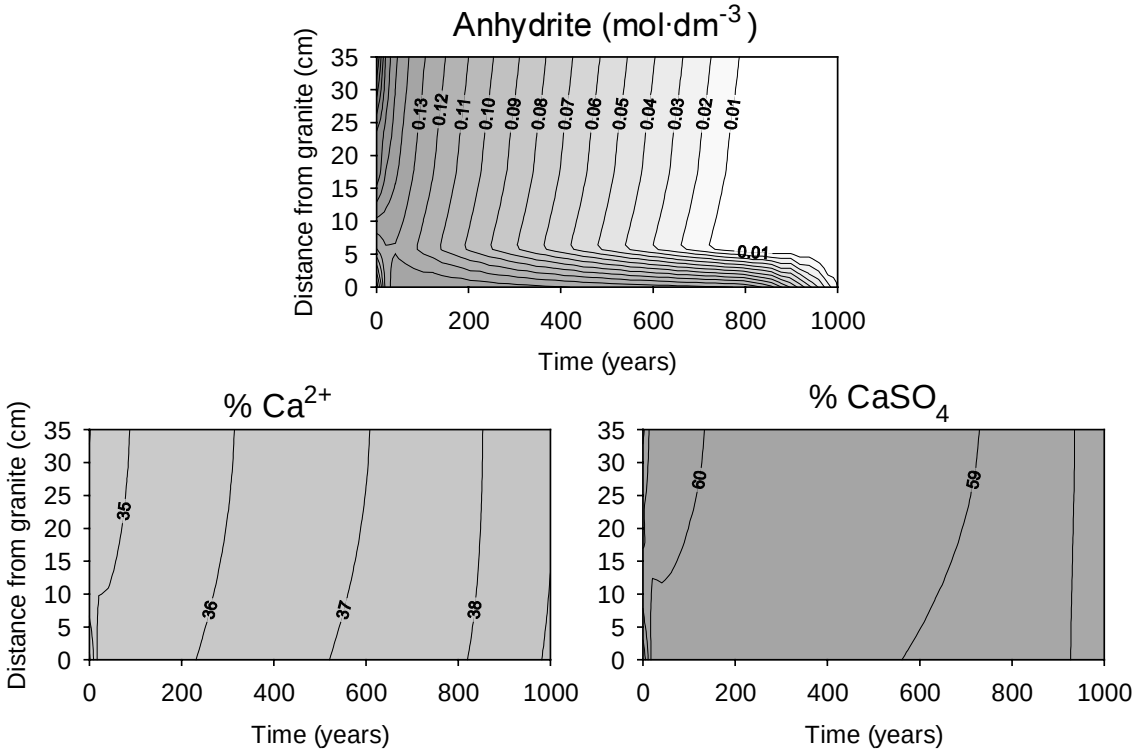

Figure 3-17. *Anhydrite evolution and aqueous calcium speciation in Model-3 after considering the same initial conditions as in Model-2.*

4 Conclusions

The results from these calculations indicate the feasibility of the modelling approach to model the migration of bentonite accessory minerals and relevant aqueous species throughout the thermal gradient. These calculations indicate that the migration of quartz and quartz polymorphs is a lesser problem.

The main process affecting the trace mineral behaviour in bentonite is cation exchange. This process controls the concentration of calcium, which results in a direct control of the calcite precipitation-dissolution. The behaviour of other minerals are more related to the diffusion of components through the bentonite, which is driven by the difference in concentration between Äspö groundwater and bentonite pore water. In Model-2, where instantaneous equilibrium were assumed throughout (except for the quartz reaction), the cation reaction is much faster and is completely exhausted by 1,000 years. Before this time, the cation exchange reaction dominates the system, and other geochemical processes are submitted to this one. After 1,000 years the system evolves independently of the cation exchange, as it has no further effect on the system once all of the possible exchange sites are used up. In contrast, in Model-3 the cation exchange reaction is much slower and is still taking place at 100,000 years, as can be seen from Figure 3-12, where gradients of the contours are all positive. Hence the cation exchange affects the system for far longer in Model-3, which in turn controls all other dissolution/precipitation processes considered, as was the case in Model-2 prior to 1,000 years.

The aqueous speciation of Ca in the bentonite pore water is fundamental in order to define the potential migration of anhydrite during the thermal stage. If $CaSO_4(aq)$ is the predominant aqueous species, then anhydrite dissolves at the initial groundwater migration times through bentonite. However, if Ca^{2+} is considered to be the dominant Ca species at the bentonite pore water, then anhydrite migrates towards the clay/granite interface. This is the main difference in the chemical systems considered in the three model approaches used in this work.

The alkalinity buffering exerted by bentonite is directly related to the calcite equilibrium, which buffers the pH at values between 9.1 and 9.8. The redox buffer capacity is exerted by the equilibrium with iron-bearing minerals as pyrite and siderite.

In future developments it would be extremely interesting to couple the present thermally induce accessory mineral migration to the effects of post-operational oxygen intrusion and the role of MX-80 bentonite as a redox buffer under the thermal transient. The results from the current work indicate that the modelling work is achievable and useful.

5 References

Berzins M, Furzelnad R M, 1985. A user's manual for SPRINT – A versatile software package for solving systems of algebraic, ordinary and partial differential equations: Part 1 – Algebraic and ordinary differential equations. Report TNER.85.085 Shell Research Limited.

Bruno J, Arcos D, Duro L, 1999. Processes and Features Affecting the Near Field Hydrochemistry: Groundwater-Bentonite Interaction. SKB TR-99-29, Swedish Nuclear Fuel and Waste Management Co.

Eriksen T E, Jansson M, 1996. Diffusion of I^-, Cs^+, and Sr^{2+} in compacted bentonite. Anion exclusion and surface diffusion. SKB TR-96-16, Swedish Nuclear Fuel and Waste Management Co.

Kim H T, Suk T W, Park S H, 1993. Diffusivities for ions through compacted Na-bentonite with varying dry bulk density. Waste Management, 13, 303–308.

Knutsson S, 1983. On the thermal conductivity and thermal diffusivity of highly compacted bentonite. SKBF KBS 83-72, Swedish Nuclear Fuel and Waste Management Co.

Madsen F T, 1998. Clay mineralogical investigations related to nuclear waste disposal. Clay Minerals, 33, 109–129.

Muurinen A, Lehikoinen J, Pusch R, 1994. Literature study on the microstructure of bentonite and its effect on diffusion. YJT Rep. 94-22.

Ochs M, 1997. Discussion of data uncertainties. Review of selected sorption and diffusion data of radionuclides in compacted bentonite. BMG report for SKB, August 1997.

Olin M, Lehikoinen J, Muurinen A, 1995. Coupled chemical and diffusion model for compacted bentonite. MRS Symp. Proc., 353, 253–260.

Parkhurst D L, Appelo C A J, 1999. User's Guide to PHREEQC (version 2) – A Computer Program for Speciation, Batch-Reaction, One-Dimensional Transport, and Inverse Geochemical Calculations. U.S. Geol. Surv. Water-Resources Investigations Report 99-4259.

Pusch R, Karnland O, Muurinen A, 1989. Transport and microstructural phenomena in bentonite clay with respect to the behavior and influence of Na, Cu, and U. SKB TR 89-34, Swedish Nuclear Fuel and Waste Management Co.

Ramebäck H, Albinsson Y, Skålberg M, Werme L, 1994. Release and diffusion of ^{90}Sr from spent UO_2 fuel in bentonite clay. Radiochim. Acta, 66/67, 405–408.

Rimstidt J D, Barnes H L, 1980. The kinetics of silica-water reactions. Geochim. Cosmochim. Acta, 44, 1683–1699.

Tarandi T, 1983. Calculated temperature field in and around a repository for spent nuclear fuel. SKB TR 83-22, Swedish Nuclear Fuel and Waste Management Co.

Tester J W, Worley W G, Robinson B A, Grigsby C O, Feerer J L, 1994. Correlating quartz dissolution kinetics in pure water from 25 to 625ºC. Geochim. Cosmochim. Acta, 58, 2407–2420.

Yu J W, Neretnieks I, 1997. Diffusion and sorption properties of radionuclides in compacted bentonite. SKB TR 97-12, Swedish Nuclear Fuel and Waste Management Co.